# Reynolds-stress and triple-product models applied to a flow with rotation and curvature

**Michael E. Olsen***

*NASA Ames Research Center, Moffett Field, CA 94035*

**Turbulence models, with increasing complexity, up to triple product terms, are applied to the flow in a rotating pipe. The rotating pipe is a challenging case for turbulence models as it contains significant rotational and curvature effects. The flowfield starts with the classic fully developed pipe flow, with a stationary pipe wall. This well defined condition is then subjected to a section of pipe with a rotating wall. The rotating wall introduces a second velocity scale, and creates Reynolds shear stresses in the radial-circumferential and circumferential-axial planes. Furthermore, the wall rotation introduces a flow stabilization, and actually reduces the turbulent kinetic energy as the flow moves along the rotating wall section. It is shown in the present work that the Reynolds stress models are capable of predicting significant reduction in the turbulent kinetic energy, but triple product improves the predictions of the centerline turbulent kinetic energy, which is governed by convection, dissipation and transport terms, as the production terms vanish on the pipe axis.**

## Nomenclature

| | |
|---|---|
| $M_\infty$ | free stream Mach number |
| $R$ | pipe radius (reference length) |
| $R_{ij}$ | Reynolds-stress tensor $\left[= \overline{u_i^{'} u_j^{'}}\right]$ |
| $Re_\tau$ | wall shear Reynolds number $[= u_\tau R/\nu_w]$ |
| $S_{ij}$ | strain rate tensor $\left[= \frac{1}{2}\left(\frac{\partial u_i}{\partial x_j} + \frac{\partial u_j}{\partial x_i}\right)\right]$ |
| $T_{ijk}$ | Turbulent transport tensor $\left[= \overline{u_i^{'} u_j^{'} u_k^{'}}\right]$ |
| $U_\infty$ | free stream velocity |
| $V_w$ | pipe wall rotation velocity |
| $\Omega_{ij}$ | rotation rate tensor $\left[= \frac{1}{2}\left(\frac{\partial u_i}{\partial x_j} - \frac{\partial u_j}{\partial x_i}\right)\right]$ |
| $\mu$ | molecular viscosity |
| $\mu_T$ | eddy-viscosity |
| $\nu$ | kinematic viscosity $\left[= \frac{\mu}{\rho}\right]$ |
| $\omega$ | specific dissipation rate $\left[= \frac{\varepsilon}{\beta^* k}\right]$ |
| $\overline{u_i^{'}}$ | Favre average Cartesian velocity fluctuation components |
| $\overline{u_i}$ | Favre average Cartesian mean velocity components |
| $\rho$ | mass density |
| $\tau_w$ | wall shear in fully developed pipe flow region |

*Research Scientist,Aerothermodymamics Branch, NASA Ames Research Center, Associate Fellow AIAA

| | | |
|---|---|---|
| $k$ | turbulent kinetic energy per unit mass | $\left[= \frac{1}{2}\overline{u_i' u_i'}\right]$ |
| $\varepsilon$ | homogeneous turbulence dissipation per unit mass | $[= \beta^* k\omega]$ |
| $a$ | sound speed | |
| $p$ | static pressure | |
| $r$ | distance from pipe centerline | |
| $u_\tau$ | friction velocity in fully developed inflow region (reference velocity) | $\left[= (\tau_w/\rho_w)^{\frac{1}{2}}\right]$ |
| $u_i$ | instantaneous Cartesian velocity components | |
| $x$ | axial distance, origin at spin/no-spin interface | |
| $x_i$ | Cartesian position coordinates | |

*Subscripts*

| | |
|---|---|
| $\tau$ | using fully developed region friction velocity as reference |
| $w$ | evaluated at the wall, $r = R$ |

## I. Introduction

Accurate computational flowfield predictions are essential for both design and operation of aerospace vehicles. As computer speeds and memory size continue to increase, Computational Fluid Dynamics (CFD) can be used to not only predict the flowfield around simple configurations, but also complete vehicle configurations. The advances in computer clock speed and memory capacity have allowed the modeling of turbulent flow, at least at lower Reynolds number, using Direct Numerical Simulations (DNS). Large Eddy Simulations (LES) continues to be developed for application to higher Reynolds numbers, but for complex configurations, DNS or even LES are still impractical because the grid required (in both time and space) is well beyond current computational capabilities.

Reynolds-stress turbulence models were envisioned to overcome a number of shortcomings evident in simple Boussinesq eddy-viscosity models. Although Reynolds-stress models have had a long history of development,[1,2] they have had, until recently, limited success in actually overcoming these limitations in practice. Reynolds-stress models have enjoyed a resurgence in the past few years,[2–4] with one new methodology incorporating the desired flow history effects on the Reynolds-stress tensor in a formulation that is numerically robust.[5,6] This Lag methodology allowed a further expansion of the flow history to include triple velocity products in a bid to obtain more accurate and complete turbulent transport predictions. This new model,[7] denoted "TTR" for Turbulent TRansport, augments the second-moment predictions of the Lag Reynolds-stress models adding field equations for the third-order-moments. These are an attempt to fulfill the need for turbulent transport predictions in regions of separation, where their relative importance is larger than it is for attached flows.

The flowfield that is studied in the present paper is not a separated flowfield, but it does includes a large central core region where the turbulent production is no longer a dominant term, and the balance of convection, transport and dissipation govern the evolution of the turbulent kinetic energy. This flowfield[8–11] is a twist on a fully developed pipe flow - literally. A fully developed pipe flow encounters a step change in the wall boundary condition, a rotating pipe wall. This introduces a set of remarkable changes in the flowfield, the most striking of which is a *reduction* in the turbulence levels as the flow traverses the rotating wall region.

The genesis of the present study was to find a simpler, less computationally intensive flowfield than the Chow-Zilliac wingtip vortex[12,13] which would allow evaluation of a flow with significant rotation, but on a simple, easily simulated geometry. The rotating pipe is a more challenging flowfield than it would appear, and it did change the formulation of the TTR model, requiring

an adjustment of the parameter governing the simple gradient diffusion of $k$ : $\sigma_k = 0.3$ (from the original 0.2).

The simulations done here were compared with simulations done in an incompressible flow code[14] using the SST turbulence model, as the turbulence model implementation could be verified to be identical using the Turbulence Modeling Resource[15] (TMR). That comparison is ongoing, and at this point the results are within 2% for axial velocity in the non-spinning section, and much better for the circumferential velocity comparison for the highest spin case studied here. This comparison between codes engendered a relatively full investigation of computational sensitivity, the highlights of which are reported here.

## II. Experiment Description/Computational Methodology

### II.A. Experiment

The Zaets[8,16–18] experiment is a low Mach number flowfield in a circular cross section pipe with a radius $R = 0.03\,\mathrm{m}$. High pressure air is supplied to a heater upstream of the pipe which brings the fluid to "room temperature" before it enters the pipe entrance through a contraction section. This temperature controlled, effectively atmospheric pressure air traverses a $200R$ length non-spinning circular pipe followed by a $50R$ section which is spinning at a wall speed of 6 m/s, 3 m/s, or 1.5 m/s – 60%, 30%, or 15% of the nominal exit centerline axial velocity (10 m/s).

The experimental measurements were obtained with DISA hot wires, single and X-wire configurations, with a 1.25 mm(=0.041 $R$) long, 5 µm diameter sensing (and hence spatially averaging) region for the quantities reported here. Analog signal linearizers were used, along with FM magnetic tape to store the signals for subsequent processing. There are measurements reported in this dataset of spectral content, with enough spatial and temporal resolution (using a different set of sensing hot-wires) to give estimates of the dissipation.

Rather than use the centerline velocity of the flow as the scaling velocity, which will vary with turbulence model, the friction velocity of the non-spinning inflow section, $u_\tau = 0.435\,\mathrm{m/s}$, was matched to the experimentally reported value for the non-spinning data. Matching this friction velocity, or more precisely the Reynolds number based on this velocity $Re_\tau = u_\tau R/\nu_w$ will match the pressure gradient in that section of the pipe, and was originally thought to provide the most unambiguous match of the experimental conditions, as each turbulence model will give very different predictions of the centerline axial velocity after traversing fifty radii of spinning wall.

The spin rates were fixed to match the ratio of the friction velocity, $u_\tau$ to the well known experimental rotation rate, so that the rotation wall speed becomes $V_w = 13.\overline{8}u_\tau$ or $V_w = 3.47\overline{2}$. The value of $Re_\tau = \frac{u_\tau R}{\nu_w}$ is reported as 875,[18] and this was the Reynolds number matched for the bulk of these simulations. Room temperature was reported as 15 °C-18 °C, and for the present paper, $288.15\mathrm{K} = 15\,^\circ C$ was used. As will be seen from the computations, the pressure and temperature in the pipe are essentially the lab pressure and temperature, and the pressure gradient inducing the flow is a pressure difference that is about 0.1% of the exit pressure, a much smaller variation than the day to day pressure variations due to weather. Though this seems like an inconsequential difference, it translates directly into Reynolds number variation, and the magnitude of this variation is easily ±3.5%, so the value reported for $Re_\tau = 875$ should really be $Re_\tau = 875 \pm 30$.

The fully developed region friction velocity was not the parameter held constant in the experiments, but rather the centerline axial velocity at the exit plane ($x = 50R$), held to roughly 10 m/s for all spin rates. A single solution for the highest spin case ($V_w = 6\,\mathrm{m/s}$ was obtained for the TTR model matching the Reynolds number $Re_0 = u_0 R/\nu_w$, where $u_0$ is the centerline axial velocity at $x = 50R$. The TTR model was chosen because it matches the experimental data best of those considered in this paper, and for that model the resulting value of $Re_\tau = 905$ at $x = -10R$. The

$u/u_\tau$ and $k/u_\tau^2$ profiles are nearly identical in the non-rotating inflow region for these two values of $Re_\tau$. At the outflow plane, the axial and circumferential mean velocity predictions are very similar, but the outflow $k/u_\tau^2$ is notably higher for the higher $Re_\tau$ simulation. This implies that the use of a single value for $u_\tau$ is not strictly accurate in comparing different spin rates. At the highest spin rates reported here, the spin rate ratio $V_w/u_\tau$ differs by 3.4% between the two simulations.

At this point, the uncertainty in knowledge of the actual Reynolds number of the flowfield from variations in atmospheric pressure should be recalled, noting that the magnitude is strikingly similar. Without further information, this is common baseline of uncertainty in the non-dimensional spin rates, as well as the Reynolds number of the fully developed pipe flow initial condition. The effects of this sort of variation can be seen in the results for the high spin case, at least as far as the solution for that turbulence model are valid.

These two Reynolds number uncertainties are not equivalent. For a fixed $Re_\tau$, increases in the spin rate (either in $V_w/u_0$ or $V_w/u_\tau$) will increase the ratio of $u_0/u_\tau$. This implies that for a fixed $Re_0$, the experimental condition, the value of $Re_\tau$ in the fully developed region will be lower than it is for the non-spinning case, with the same $Re_0$. Given a turbulence model that reproduces the physics exactly, matching the value of $Re_0$ at the spin exit will match the inflow conditions exactly, including $Re_\tau$ in the fully developed region. Having an identical inflow condition for the rotating section is necessary to be able to compare the behavior of the different turbulence models, and so $Re_\tau = 875$ in the fully developed stationary wall region is used for all spin rates. The actual $Re_\tau$ for the different spin rates discussed in the present work are probably within the 3.5% range of the $Re_\tau = 875$ used here.

## II.B. Computation

### *II.B.1. Grid*

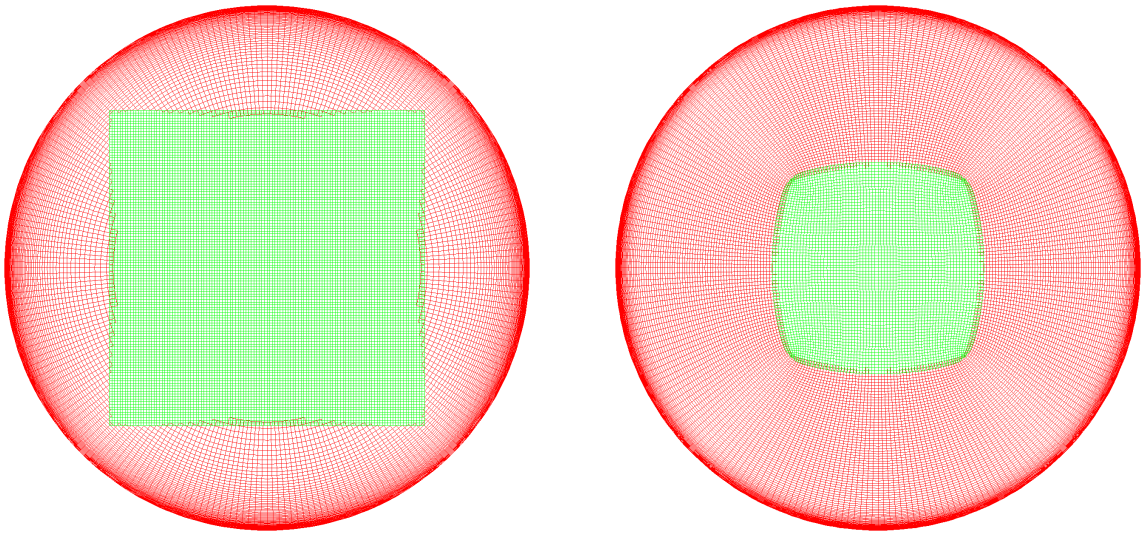

(a) overset (b) patched

Figure 1: Grid slice

Full 3D simulations were used to simulate this flowfield. The domain was broken in two, with the central core containing the axis removed and replaced by a central, essentially Cartesian, grid.

Solutions on two versions of this grid system were compared (Fig. 1), one that had a truly Cartesian central core, utilizing the full capabilities of the overset grid capability of OVERFLOW (Fig. 1a). The second grid system (Fig. 1b) has a subset that is a pointwise matched grid system that could be run without overset. The answers on these two grid systems were extremely similar, with the radial grid sensitivity essentially identical between the two systems. The differences between solutions of either overset choice were much smaller than the differences between two solutions of either overset type with a change in the radial grid density. Given this non dependence on the overset choice, the "patched" grid is used for all the results in this paper, as this grid system can be run and then compared with a solver which does not have overset capability.

The baseline viscous wall grid is 1275 (axial) $\times$ 257 (circumferential) $\times$ 121 (wall normal). The baseline core grid has the same axial distribution, and is 65 $\times$ 65 in the region which does not overlap the wall normal grid. There are 4 additional planes on either side for overlap, so the final core grid is 73 $\times$ 73 in the non-axial directions. This gives a wall normal overall grid is 154 points from the wall to the pipe axis (121+32 points). Recall that the axial extent is over $150R$, so even though there are more that 8 times more points in the axial direction, the final axial grid spacing is $0.4R$, so even at the pipe core, the grid is non-isotropic even at the pipe core, with an average axial grid spacing hundreds of times the wall normal/circumferential direction.

The near wall grid spacing was chosen as $20 \times 10^{-6}R$ with the desire to have $\Delta y^+ \leq 0.06$ when the grid was coarsened by a factor of 4, which implies that the finest grid should have $\Delta y^+ < 0.015$. This is based on the known sensitivity of the $k-\omega$ models[19] and the axial spacing was based upon earlier practice with incompressible models for this flowfield. Circumferential spacing was based on having a nearly isotropic spacing in $y$ and $z$ in the center core grid.

### *II.B.2. Numerical Method*

The code used in this study was a modified version of OVERFLOW 2.2k.[20,21] The modifications included the addition of Lag, Lag-$R_{ij}$, and TTR models along with the high speed modifications.[22] Matrix dissipation was used with smoothing parameters as recommended by earlier studies of high-speed flows with this code[22] with one critical change. Matrix dissipation[23] is appropriate for these flowfields. It combines the ability to provide accurate flowfield predictions on flows containing high normal Mach number shocks (not seen in the flowfields of this paper), while providing a low dissipation central difference scheme for the smooth regions of the flowfield. These flowfields have some discontinuous boundary conditions, but are characterized by smooth solutions over most of the problem domains. One distinct advantage of this method is the effect of the numerical dissipation can be easily assessed, since the amount of numerical dissipation is controlled explicitly.

The critical difference in the matrix dissipation smoothing parameters used is that the eigenvalue limiters are set to zero. The HLLC scheme, as coded in OVERFLOW,[24,25] is compared with the matrix dissipation scheme, and agrees with the modified matrix dissipation scheme on the coarser grids where numerical dissipation is relatively large. On the baseline grid for this paper, the difference in solutions between the standard smoothing schemes is small on the baseline grid, but becomes appreciable on the coarser grids. For clarity, the limiters are set to zero for the results in this paper. The ability to assess the influence of numerical dissipation with the matrix dissipation is extremely useful in this context.

The Pulliam-Chaussee diagonal scheme,[26] with variable time stepping or a constant Courant number (CFL) and multigrid sequencing was used as the relaxation method. For this flowfield, five levels of multigrid were used to accelerate convergence, both with grid sequencing (full multigrid in the OVERFLOW parlance) and in converging the solution at the finest level. There was an appreciable speedup in convergence even switching from four to five levels of multigrid for the SST model, which was used as the testbed for assessing solution strategy. Solutions were converged

to well over six orders of magnitude of residual reduction, and a separate check of the mass flow constancy was done to verify convergence of the individual solutions. All of the Reynolds-stress models as well as the TTR model would allow over ten orders of mean flow residual reduction, but the changes in the solutions were inconsequential after obtaining a six order reduction.

The low Mach preconditioning available in OVERFLOW[27] is crucial for simulations of this experiment. The Mach number is low enough that preconditioning is required to provide accurate solutions. If the Mach number in the pipe were increased from $M = 0.03$ to $M = 0.2$, the pressure gradient which drives the flow would also have to increase to reach the same flow Reynolds number. This pressure gradient then introduces a concomitant density gradient along the pipe's length which precludes a simple scaling of the compressible and incompressible results. The scaling would involve something akin to Favre-averaging for comparison of the incompressible and compressible flowfields.

In general, spatial convective terms and diffusion terms were all second-order accurate. For the modeling of the convection terms of the turbulence models, second order upwind was used on all the Reynolds Averaged Navier Stokes RANS models with the exception of all the Spalart-Allmaras based models. The Lag methodology does require second order accuracy (or better) since the field equations defining the lagged turbulent variables are a balance of convection and source with no diffusion terms by design–purely hyperbolic equations to accurately mimic the history effects so clearly evident in turbulent flow. In the turbulent transport level equations, not all the equations are purely hyperbolic, but they are all more driven by convection terms than standard one or two equation models.

### *II.B.3. Turbulence Models*

For this paper, two baseline Reynolds stress models are investigated. The first Reynolds stress model is the original Lag-$R_{ij}$ model[5] (referred to as the Lag-$R_{ij}$(B) model in this paper), whose equilibrium Reynolds stress assumption is the Boussinesq stress-strain assumption. The second model Lag-$R_{ij}$ Reynolds-stress model is the "926(Redistribution)" model[6] (hereafter referred to simply as the Lag-$R_{ij}$ model, that is without the (B) modifier), reproduces the commonly accepted, but overly simplistic, $4 : 2 : 3$ normal stress ratios for the flat plate boundary layer. There are experimental results[28–32] which show the much more complex behavior of the Reynolds stresses in flat plate boundary layers, but the adjustment of the underlying model is not attempted, the same model as described in earlier work is retained. The triple product Lag-$T_{ijk}$ model[33] (afterward referred to as the TTR model) uses the more complex "926" stress-strain model as its $R_{ij}^{(eq)}$ stress-strain assumption, so the additional physics introduced with the turbulent transport terms are seen comparing the Lag-$R_{ij}$ and Lag-$T_{ijk}$ models. The Lag-$T_{ijk}$ model has been slightly modified from its original description (see the appendix A for the details of this model), with the only change an increase in the $\sigma_k$ parameter to $\sigma_k = 0.3$ from its original value of 0.2.

The eddy viscosity models to which these more complicated models are compared are the Lag-$\nu_T$ eddy viscosity model,[34] the "standard" Menter shear-stress transport (SST) model,[15] and the rotation and quadratic constitutive relation (QCR) and rotation correction modified Spalart-Allmaras (SA) model.[15,35,36] The implementation of these models is that of OVERFLOW, with the 2.2k version coding used, and the SST model checked directly against the TMR website[15] to ensure that its implementation was consistent with what had been verified earlier.[37]

### *II.B.4. Boundary Conditions*

The boundary equations for the turbulence model field equations are those enumerated in the original paper outlining the TTR model.[33] At viscous walls, $k$ and all $R_{ij}$ and $T_{ijk}$ components are set to zero, consistent with smooth wall conditions. $\omega$ is set to $60\mu/\left(\beta^*\rho\Delta z_0^2\right)$. For boundaries

with flow into the solution domain, $k$ is set to a $10^{-6}u_\infty^2$, and $R_{ij}$ is set to $\frac{2}{3}k\delta_{ij}$. $\omega$ is chosen to provide $\frac{\nu_T}{\nu} = 0.1$. All $T_{ijk}$ components are zero at far field inflow boundaries. For boundaries with flow out of the domain, all turbulence quantities are simply extrapolated.

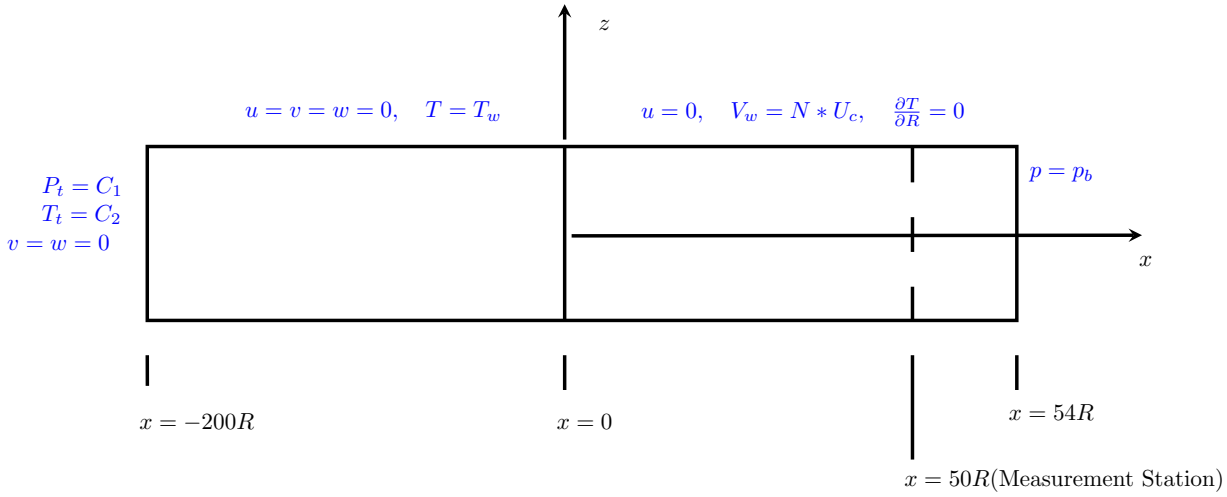


Figure 2: Boundary conditions and $x$-$z$ plane configuration

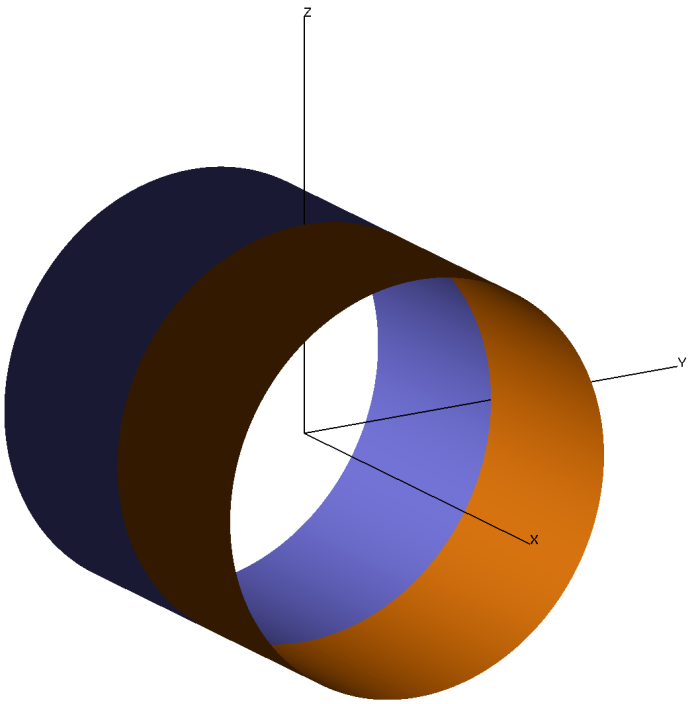


Figure 3: Geometry
(near spin/no-spin interface)

The boundary conditions that are imposed on the other variables for this particular flowfield are shown in Fig. 2. The viscous walls are boundary conditions are isothermal no slip on the upstream non-spinning section, and adiabatic no slip on the spinning downstream section. The wall boundary temperature was chosen to be equal to the inflow static temperature, though it will be seen in the results that the low Mach number of this flowfield ensures that the temperatures are essentially constant within the entire domain, so adiabatic walls throughout would be equally viable, and would give indistinguishable results. Constant total pressure and total temperature with axial flow ($v = w = 0$) is imposed at the inflow plane, with the static pressure allowed to vary. Static pressure is the only quantity imposed at at the outflow plane, and this value is chosen to obtain $Re_\tau = 875$ in the fully developed stationary wall region just upstream of the spinning wall section. The back pressure choice is slightly different for each turbulence model, depending on the pressure variation predicted in the rotating wall section of the pipe depends on the turbulence model.

The domain simulated was chosen with an eye to allow reproduction by other flow codes, so

the full upstream development section was simulated. The results shown in this paper are taken from the fully developed region of the stationary pipe section. This position was chosen to be $X = -10R$, as this was upstream of the disturbances created by the onset of the wall spin. Indeed, profiles anywhere in this region are essentially identical, as this is fully developed pipe flow. The $X = -10R$ point was also where the computational value of $u_\tau$ was determined. The downstream domain was extended to $x = 54.8R$, slightly beyond the $x = 50R$ location where the profiles are compared with experiment, so that any boundary condition inconsistencies were eliminated from the profile comparisons. As there is substantial turbulent kinetic energy as well as radially varying circumferential velocity in this portion of the flowfield, a truly fixed static pressure along the back face is not a completely consistent downstream boundary condition, but the anomalies created by these small discrepancies are eliminated with a slightly extended domain, and will be more easily simulated by other flow solvers.

In this paper, the convention chosen is that the solution is described for the plane $y = 0$. The "1" direction is $x$, the axial direction. The "2" direction is $y$, and for the plane $y = 0$ is the circumferential direction. The "3" direction is $z$, wall normal. The $z$ spatial direction is called $r$, which makes obvious the axisymmetric nature of the geometry. Thus the circumferential velocity is $v$, and the axial Reynolds-stress is $R_{11}$. The circumferential Reynolds-stress is $R_{22}$, and the wall-normal Reynolds-stress is $R_{33}$.

# III. Results

## III.A. Overview and Solution Sensitivity

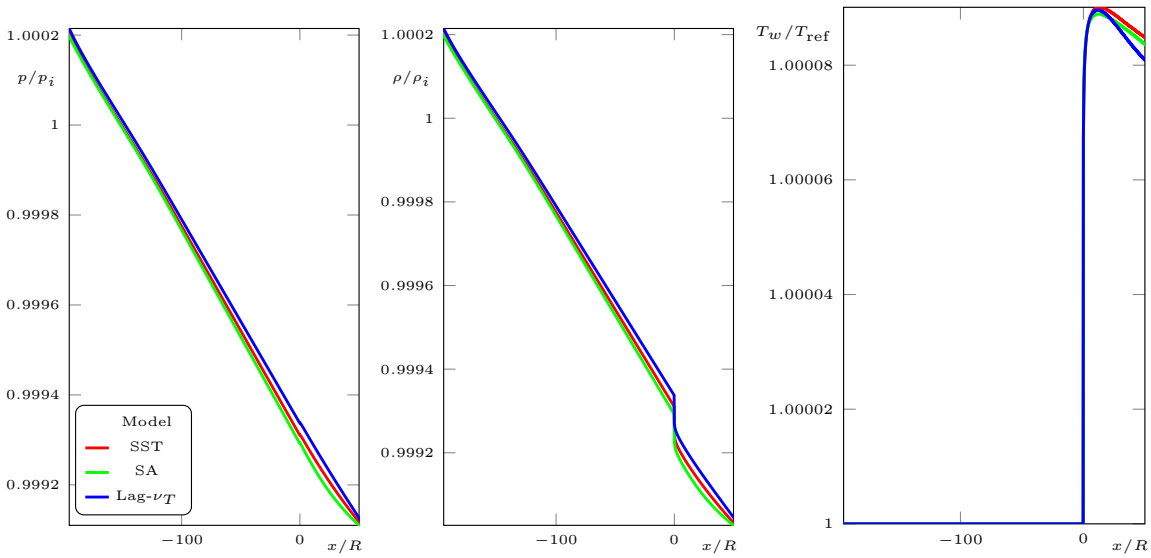


(a) pressure (b) density (c) temperature

Figure 4: Rotating pipe wall surface conditions - eddy viscosity models

For the nominal value of $Re_\tau = 875$, the pressure, density, and temperature on the wall of the pipe (Fig. 4) have minuscule variation from the inlet conditions: pressure and density variations are less than 1 part in 10,000. The temperature, whose variation over the upstream portion of the pipe is held constant varies by less than 1 part in 100,000. One of the more intriguing aspects of this variation is the behaviour of the density at the start of the spinning section. The steep (albeit diminutive) rise in temperature at the interface is consistent with the increased viscous

dissipation with the introduction of the spin, and as pressure is smooth (as it has to be) in the converged solution, the temperature rise is matched with a corresponding density drop. Though an interesting feature, the magnitude of these variations makes their influence on the solution inconsequential.

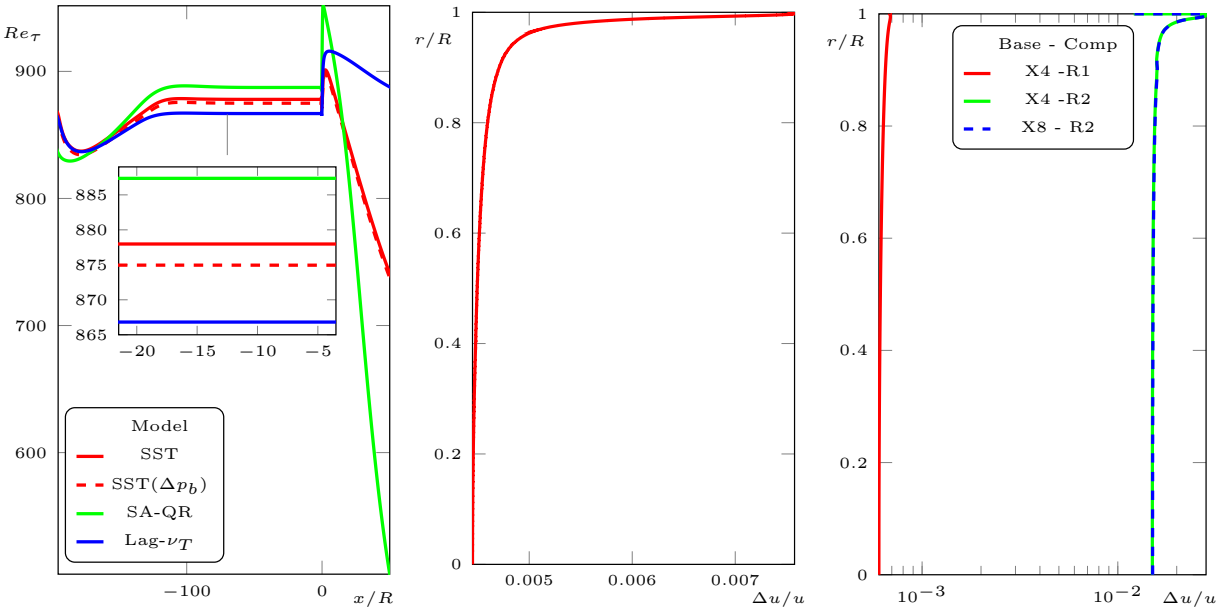


(a) $Re_\tau$ Distribution (b) $Re_\tau$ sensitivity (0.7% change) (c) Axial/Radial Grid Coarsening

Figure 5: $Re_\tau$ distribution and axial velocity sensitivities (SST model) to small $Re_\tau$ changes and grid coarsening

The flowfield can be thought of as an upstream fully developed pipe flow (the non-rotating section) which has essentially a single parameter to be matched, the value of $Re_\tau = \frac{u_\tau R}{\nu_w}$, which is governed by the downstream pressure choice. In the fully developed portion of the upstream section ($-80 \leq x/R \leq 0$), the wall shear is balanced by the pressure gradient. The constancy of this wall shear, or equivalently the pressure gradient, can be seen in Fig. 5, which shows results for three eddy viscosity models for the same choice of the downstream static pressure. The experimental value of this parameter in the non-spinning, fully developed pipe flow region just upstream of the spinning section is ($Re_\tau = 875$). These solutions are close to matching the experimental $Re_\tau$, but do not exactly match. Since each turbulence model gives a different pressure behavior in the spinning section, each model requires a adjustment of the downstream pressure to match the $Re_\tau$.

The inset plot in Fig. 5a shows a detail of the $Re_\tau$ distribution, and the dashed lined line shows the $Re_\tau$ distribution for the SST model with the back pressure adjusted to match $Re_\tau = 875$ in the fully developed region. The original $Re_\tau$ (denoted by the solid line) is 878, a difference of 0.8% in $Re_\tau$. The effect of this difference in the axial velocity solution for this change in $Re_\tau$ is shown in Fig. 5b, and the magnitude ($\approx 0.7\%$) is roughly equal to the magnitude of the discrepancy in $Re_\tau$. This implies that the $Re_\tau$ must be matched relatively closely to be able to correctly distinguish differences due to other changes, such as turbulence model choice, flux method choice, etc., even if the actual value of this parameter is known with much less precision. An assessment of effect of a 3.5% variation in $Re_\tau$ for the TTR model will be documented for the highest spin case, and this level of variation does make a difference.

Fig. 5c shows the relative changes in the axial velocity for three different grid coarsenings. The effect of coarsening the axial spacing by a factor of four (red line), leaving the radial spacing

unchanged is less than $.0007u(r/R)$, that is it is *uniformly* less than this fraction of the *local* axial velocity, even close to the wall. By comparison, coarsening axially coarsened grid by a factor of 2 in the radial direction ( green line) results in a uniform fractional change that is (again *uniformly*) less than $0.003u(r/R)$ of the local velocity. In other words, the effect of a single radial coarsening is more than ten times that of a double axial coarsening. Then doing a further axial coarsening (blue line) gives no appreciable change in the solution - the changes from the single radial coarsening still swamps the effects of an eightfold axial coarsening. Apparently a more efficient grid for this case would be finer radially, and coarser axially.

### III.B. Non Spinning (Fully Developed) Flow

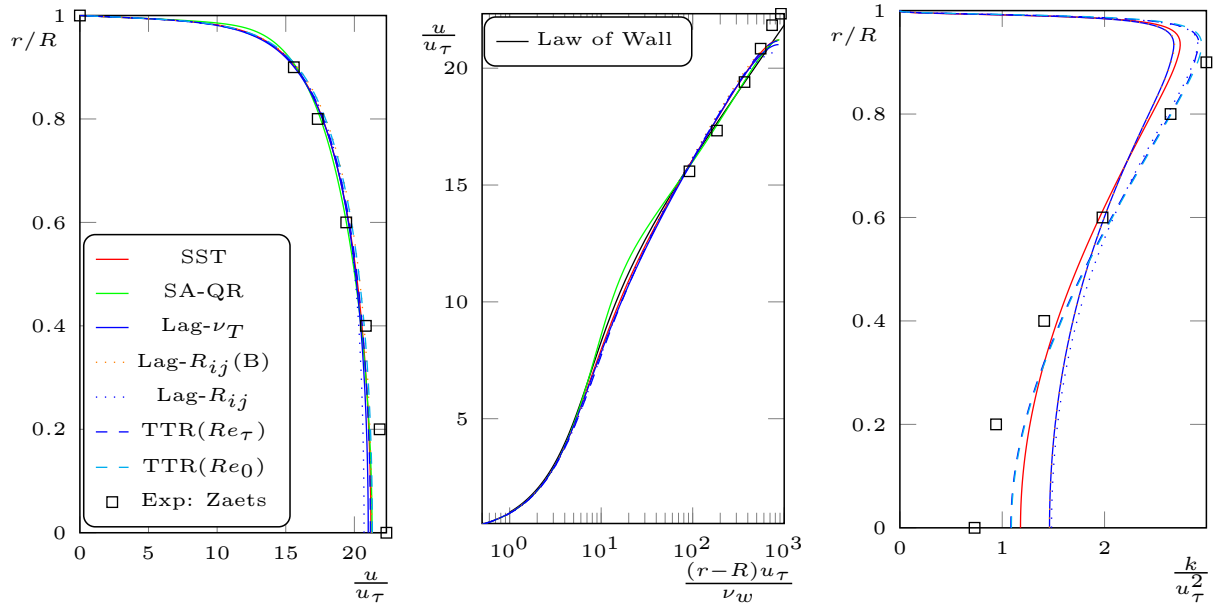


(a) Axial Velocity Outer Variable $(r/R)$

(b) Axial Velocity Inner Variable ($u^+$ vs $y^+$)

(c) Turbulent Kinetic Energy

Figure 6: Inflow velocity and $k$ profiles$(x/R = -10)$

Profiles of the fully developed region just upstream of the start of the spinning section are shown in Fig. 6. This is in effect an initial condition for the evolution of the flow that will occur in the rotating section of the pipe, and since it is fully developed pipe flow, it is a relatively computationally stable condition for any of these turbulence models, in that the profiles of velocity, $k$ , or any other flow quantity are extremely similar at any axial location within the range $-80R \leq x \leq -5R$. The inflow axial velocity is shown in Fig. 6a, and these are the axial velocity profiles for fully developed pipe flow at $Re_\tau = 875$ for all of the turbulence models presented in this paper. All the models agree with each other at this point in the flowfield, as might be expected since they were all tuned to give similar results for flat plate flows. This is a relatively low Reynolds number flowfield, as can be seen in the law of the wall subplot (Fig. 6b), with a minimal "log" region.

The turbulent kinetic energy profiles in the entrance region (Fig. 6c) highlights some of the characteristics of the various Lag models. All three agree in the near wall region, with the differences between these where production vanishes near the centerline. Indeed, only at the centerline, where production is zero, and turbulent transport is balanced only by dissipation (in the fully developed region) or by dissipation and convection (in the rotating wall region) are there appreciable differences between the TTR model and the non-Boussinesq Lag-$R_{ij}$ on which it is based.

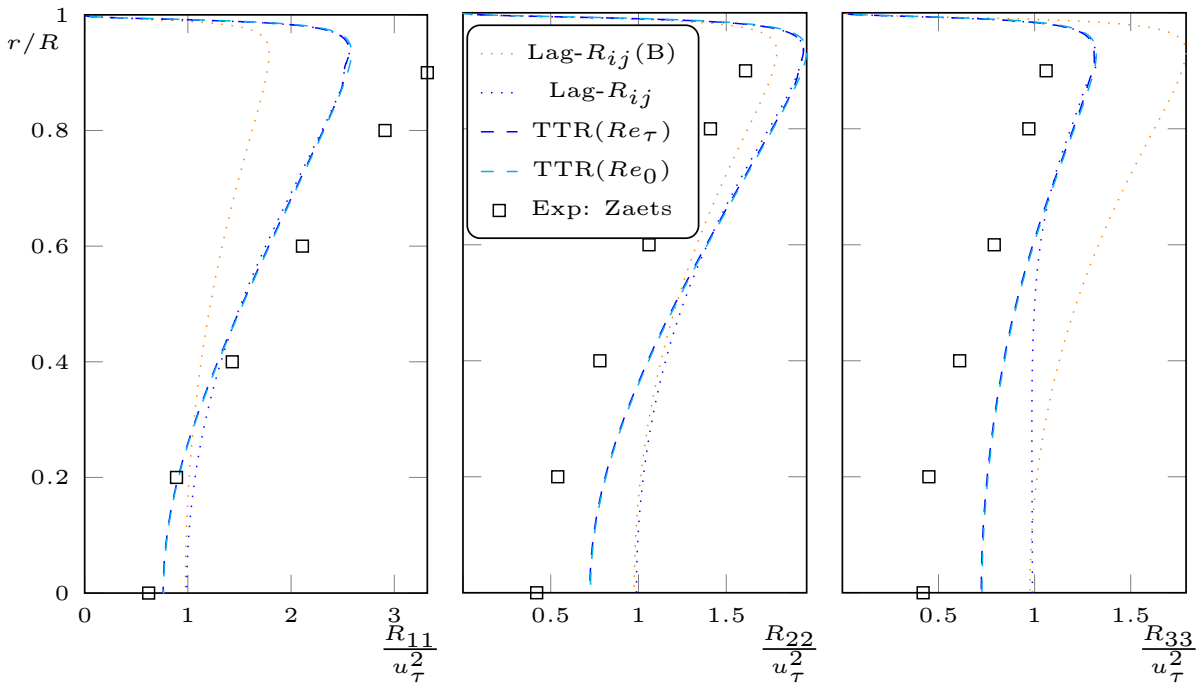


(a) $R_{11}$ (b) $R_{22}$ (c) $R_{33}$

Figure 7: Inflow normal Reynolds-stress profiles ($x/R = -10$)

One additional point to be taken from Fig. 6 is the second solution plotted for the TTR model, where the $Re_0 = u_0 R/\nu_w$ was matched to the experimental value, rather that matching $Re_\tau = 875$. For the axial velocity (in either plot), the differences between the two conditions are hard to distinguish - the differences are minute. Even the turbulent kinetic energy (non-dimensionalized by the correct value of $u_\tau$ for each simulation) shows no significant difference. In the fully developed inflow, when non-dimensionalized by the friction velocity, the flow has a very small change for this level of Reynolds number variation.

Another quantity that can be compared at this point is the turbulent kinetic energy, and for the actual axial Reynolds stress models, the normal stresses $R_{11}$, $R_{22}$ and $R_{33}$. In making this comparison, the classic, and undoubtedly incorrect, tuning of the flat plate isotropy to produce the $4:2:3$ throughout the log region for the non-Boussinesq Lag-$R_{ij}$ model, which is also the basis for the TTR model should be kept in mind. The $4:2:3$ ratio is not what the experiment shows for this flow field, but the tuned anisotropy is closer to the actual anisotropies than the isotropic assumption inherent in a Boussinesq stress-strain relationship. A comparison of the Reynolds-stress predictions and measurement is shown in Fig. 7. The experimental anisotropies are higher than are predicted by the model in the near wall region, but the anisotropic stress-strain relation is closer to experiment than the Boussinesq, and the turbulent transport terms do not affect the predictions in the near wall region where production is a dominant process. However, at the pipe centerline, where production vanishes, the TTR model gives a better prediction than the baseline Reynolds-stress model. Improvement in the anisotropy predictions (which is a function of the $R_{ij}^{(eq)}$ for the bulk of the flowfield) would presumably improve all these predictions.

Again, turning to the inherent uncertainty in the actual $Re_\tau$ value in the inlet, the predictions of the TTR model show extremely small variation for this level of Reynolds number change, as would be expected. Both versions of TTR predictions for an $Re_\tau$ variation of 3.4%, give largely the same

profiles in Fig. 7. The differences in the $R_{ij}^{(eq)}$ choice and the turbulent transport modifications of the TTR are much larger than the differences induced by this level of uncertainty in $Re_\tau$.

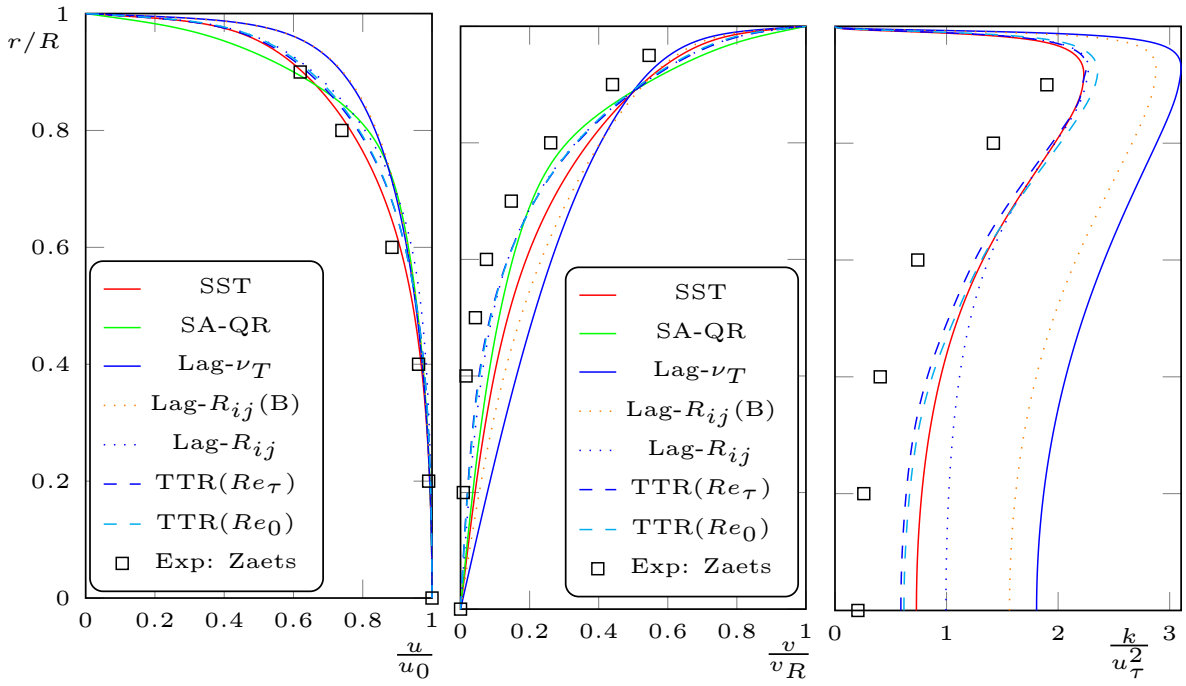


(a) Axial Velocity (b) Circumferential Velocity (c) Turbulent Kinetic Energy

Figure 8: High spin rotating section flow profiles ($x/R = 50, V_w/u_\tau = 13.8$)

### III.C. Rotating Wall Section - Fast Spin

In contrast to the inflow section, where there is relatively little difference between the turbulence model predictions, the predictions in the rotating wall region are very different for different turbulence models. The first set of results are for the most rapid spin reported in the Zaets,[8] $V_w = 6$m/sec ($\frac{V_w}{u_\tau} = 13.88$). Where vorticity production based SST and strain based production models agree in the inflow section, the vorticity based version gives dramatically different (and wrong) results in the spinning section. Similarly, the non modified SA model, with QCR and rotation correction gives dramatically wrong answers here. These dramatic fails are not shown here, it is not surprising that they have problems with this change in conditions. What was surprising was that an unmodified SST model actually did reasonably well. The SA modifications were designed to work better in flows with significant rotation, and so the improvement was less more an expected result.

The eddy viscosity Lag model has not been modified to handle rotational effects, but it did not fail as spectacularly as vorticity production based SST, or unmodified SA, but it does not predict the dramatic stabilizing effects of this rotational flow. Perhaps unsurprisingly, all the Lag-$R_{ij}$ models give better predictions than the eddy viscosity based Lag model. None of the usual Richardson number, curvature or other corrections to the underlying models have been made in any of the Lag based models, simply the introduction of more of the physical terms with increasing model complexity.

Lets start the comparison with the mean flow comparisons in Fig. 8. The axial velocity predictions (Fig. 8a) of the models are much more varied than was evident at the inflow section. The worst comparison here is the eddy viscosity Lag model, unsurprising since it has no rotation correc-

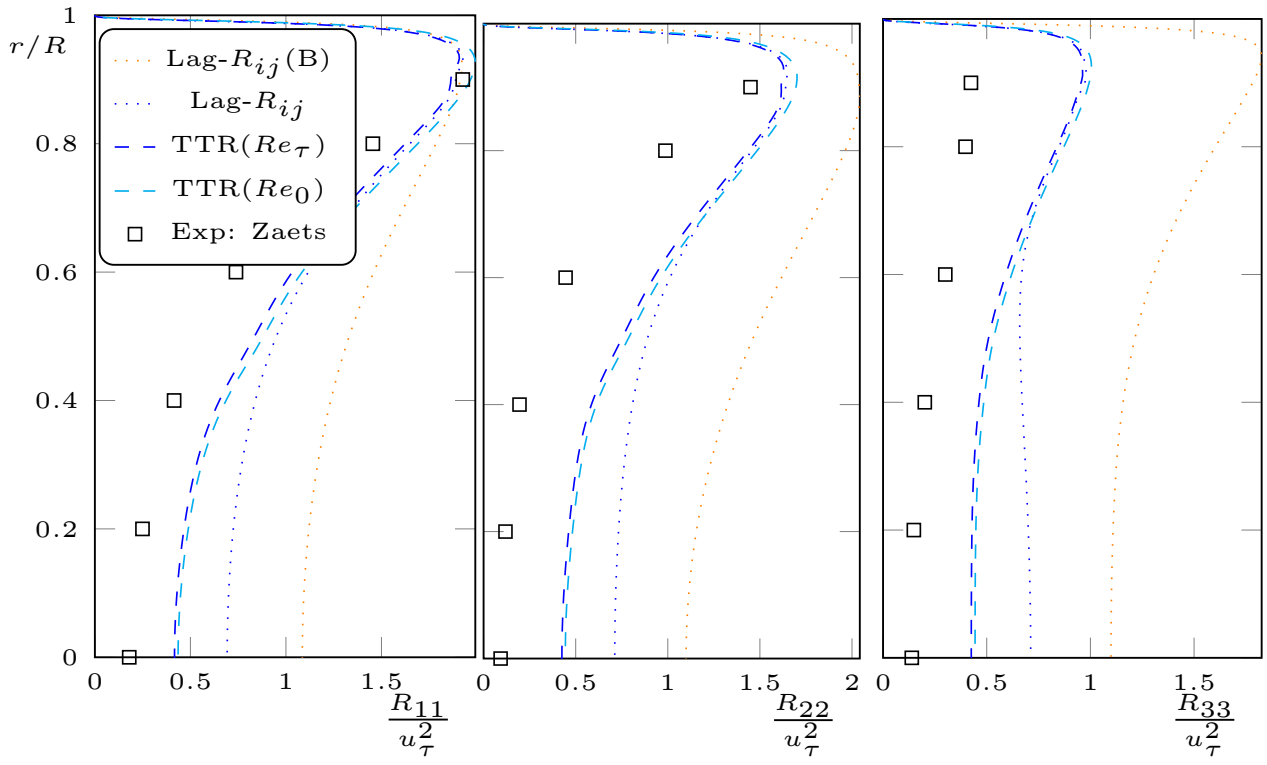


(a) $R_{11}$ (b) $R_{22}$ (c) $R_{33}$

Figure 9: High spin normal Reynolds-stress profiles ($x/R = 50$, $V_w/u_\tau = 13.\overline{8}$)

tions in its formulation. The modified SA model gives a good prediction of the centerline velocity, but misses the shape of the profile closer to the spinning wall. SST does a very creditable job in predicting the axial velocity, and the Reynolds stress models do well, underpredicting the centerline velocity in the same way they did in the inlet section. It is not clear if this is a good or bad result, as none of the models (save the Boussinesq based Lag-$R_{ij}$ model) predicted the centerline velocity at the inflow.

The circumferential velocity predictions give a different story, with the only common factor the poor prediction by the eddy viscosity Lag model. In its defense, the unmodified SA and vorticity based SST models give worse predictions for this case, and the better showing of the Lag model is probably due to the fact that it's production terms are based on the physically correct strain formulation, and not the "wall bounded flow" cheat of substituting vorticity for strain. SST actually gives a better circumferential velocity prediction than the Boussinesq based Lag-$R_{ij}$ model, but the other Lag-$R_{ij}$ and TTR models give superior predictions for this mean flow velocity.

The turbulent kinetic energy profiles for the high spin case are shown in Fig. 8c. Recall that there were modest differences in the peak $k$ values for all the models in the non-spinning inlet (Fig. 6c). At the end of the spinning section, there are large differences between the two Lag-$R_{ij}$ models in terms of the peak value of $k$ . The TTR and it's sister Lag-$R_{ij}$ model are in relative agreement for the peak value of $k$ , comparing of course the solutions with the same inlet section $Re_\tau$. Note that, in contrast with the fully developed inlet region, the $k/u_\tau^2$ profiles are different for the two TTR solutions at different inlet values of $Re_\tau$. The TTR model does provide a better match near the pipe centerline over the underlying Reynolds-stress model again. However, none of these models does predict the full extent of the drop in $k$ seen in the experiment.

One of the strengths of this data set is that there is a significant amount of data useful for Reynolds-stress model development, and Fig. 9 shows a comparison of all three normal Reynolds stresses for this case. The anisotropy is not perfectly predicted, but the general shape and relative size of the Reynolds stress profiles is captured by the TTR model. The Lag-$R_{ij}^{(eq)}$ model it is based on also does a creditable job, but the TTR model improves the predictions near the pipe centerline where turbulent transport is a more dominant term than closer to the wall.

### III.D. Rotating Wall Section - Slow Spin

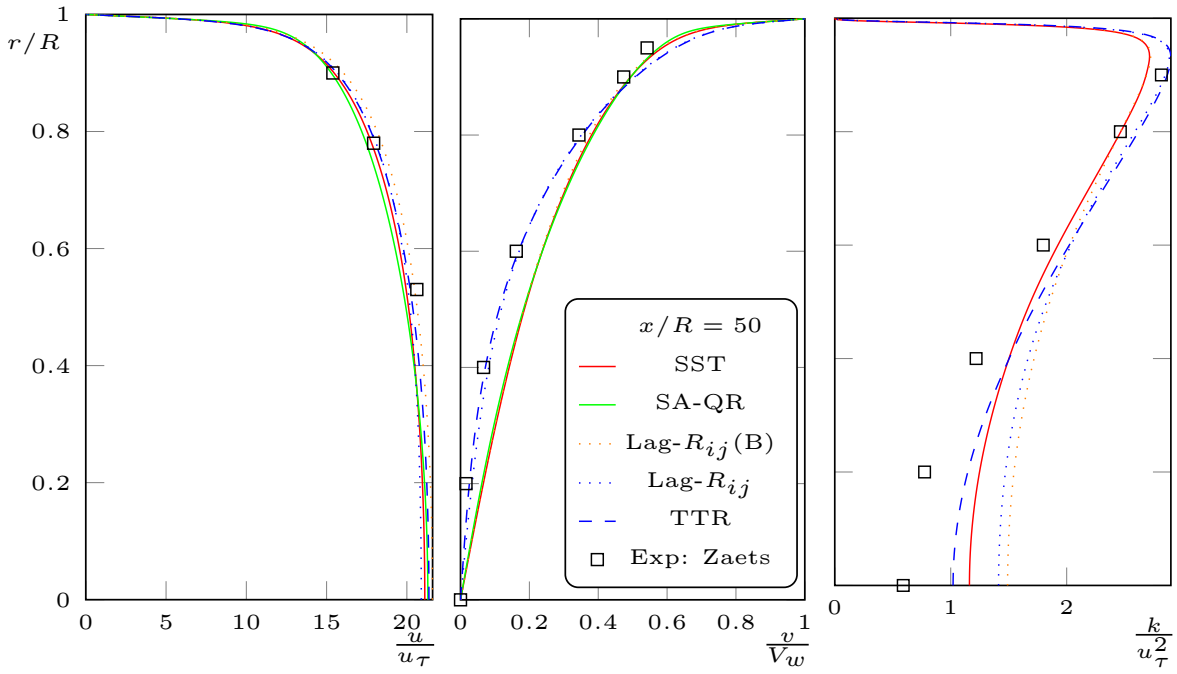


(a) Axial Velocity (b) Circumferential Velocity (c) Turbulent Kinetic Energy

Figure 10: Low spin rotating section flow profiles ($x/R = 50, V_w/u_\tau = 3.4258\overline{8}$)

Turning to the less rapidly spinning case in the Zaets[8] experiment, $V_w = 1.5$m/s ($\frac{V_w}{u_\tau} = 3.47$), the mean flow predictions for this lower level of spin in Fig. 10 are different than seen at the higher spin rate. The axial velocity is underpredicted by all the models, but the SA-QR model is now furthest from experiment. The TTR model is closest to the experiment for this case, but is pretty much in line with the other Reynolds stress and SST models. The circumferential velocity is well predicted by either the anisotropic Reynolds stress model and the TTR (which is based upon the same Reynolds-stress stress-strain equilibrium relation), but similar to the axial velocity results, the SA-QR model has now moved away from the experimental results.

The $k$ profile predictions (Fig. 10c) for the lower spin rate are also reasonably good, with the $R_{11}$ predictions much better than for the turbulent kinetic energy. The TTR model again improves the centerline prediction, but the underlying anisotropy is still less than seen in the experiment. The turbulent transport model does seem to be moving the turbulence results in the correct direction at the centerline, and does seem to have less of an effect near the wall. This is in line with what was expected and the earlier results.[7]

The normal stress predictions for the low spin case are shown in Fig. 11. Again the models with the non-isotropic $R_{ij}^{(eq)}$ are much more in line with the experimental data than the Boussinesq

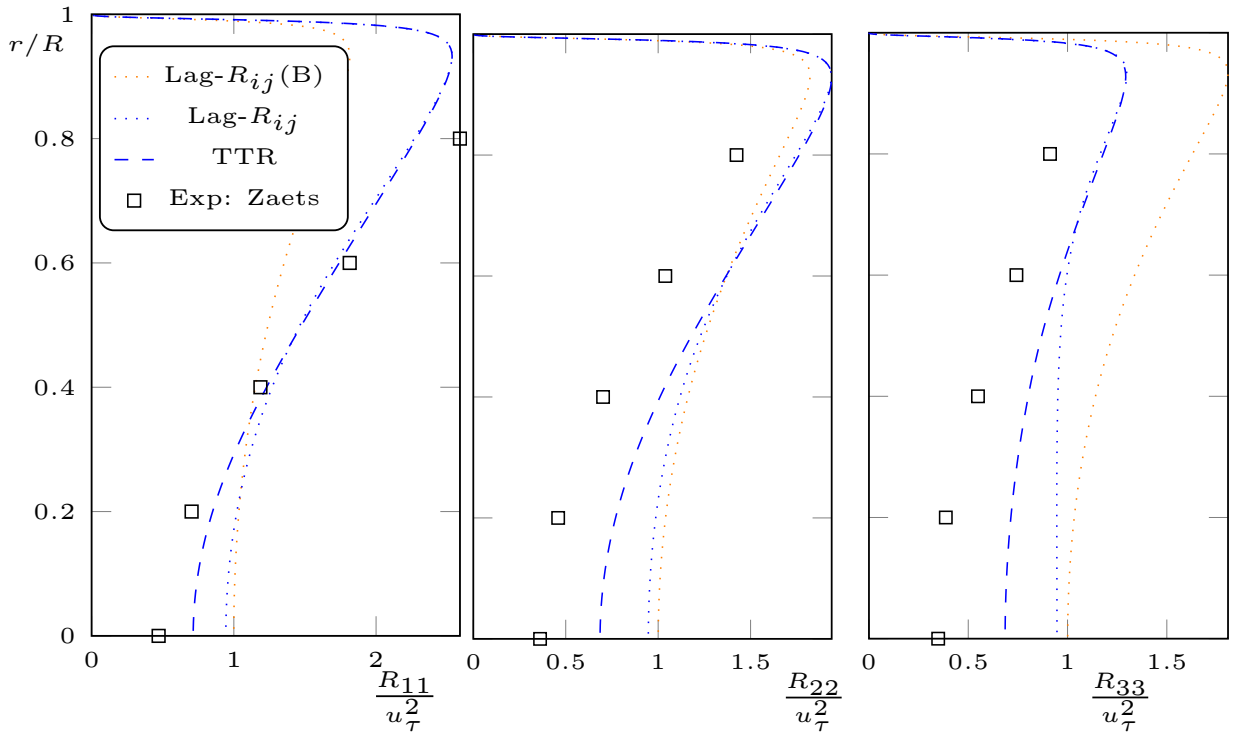


(a) $R_{11}$ (b) $R_{22}$ (c) $R_{33}$

Figure 11: Low spin normal Reynolds-stress profiles ($x/R = 50$, $V_w/u_\tau = 3.425\overline{8}$)

based Lag-$R_{ij}$ model. Furthermore, very much like the higher spin case, the TTR model provides a significantly better prediction of the normal stresses close to the pipe core, reducing the magnitude of the $R_{ij}$ levels significantly there.

## IV. Conclusions - Further Work

The TTR model improves the prediction for this flowfield over baseline Reynolds-stress model. The turbulent transport effects are more pronounced in the regions where turbulence production becomes less important, here the centerline of the pipe. In the wall region, the turbulent transport terms are of less relative importance, and the underlying Reynolds stress model predictions are recovered.

The anisotropic Reynolds-stress model produces better results than the one based on the Boussinesq stress-strain relation. Even though the anisotropy is less complex than the actual anisotropy behaviour of the turbulence is, it is an improvement over the isotropic normal stress relation.

The SST (strain production) and SA with curvature and QCR relations give better results than SST-V (vorticity production) or the unmodified SA model, the TTR and Reynolds stress models gives a better (and more complete) prediction of the flowfield. Even with this improved prediction, there is room for improvement both in the Reynolds stress anisotropies and also in the $k$ reduction brought about by the flow rotation/curvature.

Investigation of the alter ego of this flowfield, the spinning cylinder,[38,39] where the rotational effects are destabilizing, and turbulence enhancing, is ongoing, and flow invariant based versions of the Richardson number (rotation) and curvature corrections done with earlier (ad-hoc) turbulence model corrections[8–11,40] is ongoing, and initial results are promising.

A final, and important, thing to keep in mind is that the turbulence models evaluated in this paper have *not* been tuned to match this flowfield, though the SA model which is used includes both the QCR and rotation corrections. No explicit Richardson number/curvature or other corrections are applied to any of the other models. The response of the models to the effects of the rotating wall are purely those inherent in the model formulations directly. The change in the TTR model is not really a tuning to match the flowfield, but rather an acceptance that the anti-diffusive properties of the triple product turbulent transport terms had to be compensated for with the additional gradient diffusion of $k$ .

Flow invariant based versions of Richardson/curvature corrections are being evaluated, along with fixes to the equilibrium anisotropy for the Lag-$R_{ij}$ and TTR models. Regardless, the addition of the non-aligned stress-strain relation of the Lag-$R_{ij}$ and TTR models, as well as the turbulent transport improvements brought in by the TTR model improve the prediction of this flow field without these adjustments, and the improvements are not small.

## Acknowledgements

The impetus for choosing this flowfield is from the suggestions of the Turbulence Model Benchmarking Group, especially Brian Smith who suggested this specific case. Svetlana Poroseva, also a member of TMBG was of great help, with papers and data supplied from her website which greatly facilitated this work. Neil Ashton a third member is working on the same flowfield with the incompressible version of OPENFOAM, and his collaboration is greatly appreciated.

The "patched" grid system used for the rotating pipe case in the paper was created by Dinesh K. Prabhu. This grid system will allow comparison between overset capable codes and other non-overset codes, and is a valuable and much appreciated contribution to this work.

## Appendix A Third-Order-Moment Turbulence Model (TTR)

This model is built on top of the preceding Lag methodology models, and the equilibrium two equation turbulence model that is at their heart, the Wilcox 1988 $k$-$\omega$ model. The third-order-moment model comes from the exact Reynolds-stress and turbulent transport equations.

$$\begin{aligned}\partial_t\left(R_{ij}\right)+\partial_k\left(u_k R_{ij}\right) =& -R_{jk}\partial_k\overline{U_i}-R_{ik}\partial_k\overline{U_j}-\partial_k T_{ijk}+\nu\partial_k\partial_k R_{ij} \\ &+\Pi_{ij}-2\nu\overline{\partial_k(u_i')\partial_k(u_j')}\end{aligned} \tag{1}$$

$$\begin{aligned}\partial_t\left(T_{ijk}\right)+\partial_l\left(u_l T_{ijk}\right) =& -T_{ijl}\partial_l\overline{U_k}-T_{jkl}\partial_l\overline{U_i}-T_{kil}\partial_l\overline{U_j} \\ &+R_{ij}\partial_l R_{kl}+R_{jk}\partial_l R_{il}+R_{ki}\partial_l R_{jl} \\ &+\nu\partial_l\partial_l T_{ijk} \\ &+\Pi ijk-\partial_l(Q_{ijkl})-\varepsilon_{ijk}\end{aligned} \tag{2}$$

where the neglected red terms are

$$\Pi_{ij} = \frac{1}{\rho}\left[\overline{u_j'\partial_i(p')}+\overline{u_i'\partial_j(p')}\right] \tag{3}$$

$$\Pi_{ijk} = \frac{1}{\rho}\left[\overline{u_i'u_j'\partial_k(p')}+\overline{u_j'u_k'\partial_i(p')}+\overline{u_k'u_i'\partial_j(p')}\right] \tag{4}$$

$$Q_{ijkl} = \overline{u_i'u_j'u_k'u_l'} \tag{5}$$

$$\varepsilon_{ijk} = 2\nu\left(\overline{u_i'\partial_l(u_j')\partial_l(u_k')}+\overline{u_j'\partial_l(u_k')\partial_l(u_i')}+\overline{u_k'\partial_l(u_i')\partial_l(u_j')}\right) \tag{6}$$

The TTR turbulence model including turbulent transport ($T_{ijk}$) terms is:

$$\partial_t(\rho k) + \partial_l(\rho u_l k) = \rho\left[R_{ij}S_{ij} - \beta^* k\omega\right] + \partial_l\left(\left(\mu + \sigma_k\mu_T\right)\partial_l k\right) - A_4\partial_l\left(\rho T_{iil}\right) \tag{7}$$

$$\partial_t(\rho\omega) + \partial_l(\rho u_l\omega) = \alpha\rho S^2 - \beta\rho\omega^2 + \partial_l\left(\left(\mu + \sigma_\omega\mu_T\right)\partial_l\omega\right) \tag{8}$$

$$\partial_t(\rho R_{ij}) + \partial_l(\rho u_l R_{ij}) = A_0\rho\omega\left(R_{ij}^{(eq)} - R_{ij}\right) \tag{9}$$

$$\partial_t(\rho T_{ijk}) + \partial_l(\rho u_l T_{ijk}) = A_0\rho\omega\left(T_{ijk}^{(eq)} - T_{ijk}\right) \tag{10}$$

where

$$T_{ijk}^{(eq)} = \frac{A_2}{A_0\omega}\left[T_{ijl}\partial_l\overline{U_k} + T_{jkl}\partial_l\overline{U_i} + T_{kil}\partial_l\overline{U_j} - R_{ij}\partial_l R_{kl} - R_{jk}\partial_l R_{il} - R_{ki}\partial_l R_{jl}\right] + \frac{1}{A_0\rho\omega}\left[\partial_l\left(\left(\mu + \sigma_t\mu_{t_E}\right)\partial_l T_{ijk}\right)\right] \tag{11}$$

$$\mu_{t_E} = \rho k/\omega \qquad S = \sqrt{2\left(S_{ij}S_{ij} - S_{kk}^2/3\right)}$$

$$\mathcal{P} = R_{ij}S_{ij} \qquad S_{ij} = \frac{1}{2}\left(\frac{\partial u_i}{\partial x_j} + \frac{\partial u_j}{\partial x_i}\right)$$

$$\varepsilon = \beta^*\rho k\omega$$

Most of the parameters for this model are set by the requirement to retain the equilibrium predictions of the underlying $k$-$\omega$ model. The equilibrium Reynolds-stress relation is one of the three described in earlier Reynolds-stress model work,[6] denoted as the "926(Redistribution)" Equilibrium Reynolds-stress relation. This constitutive relation is most directly related to the explicit algebraic Reynolds-stress models.[41–43] The terminology is borrowed from the paper introducing this relation,[6] and contains production terms which are *not* the full Reynolds-stress production terms, but do yield log layer anisotropies consistent with the classic 4:3:2[44] relation. These "production" terms (which have really only redistribution terms, and none of the work terms of actual production) are

$$\mathcal{P}_{11} = 2\left(kS_{11}/A_1 + \left(R_{31}\,\Omega_{31} - R_{12}\,\Omega_{12}\right)\right) \tag{12}$$

$$\mathcal{P}_{22} = 2\left(kS_{22}/A_1 + \left(R_{12}\,\Omega_{12} - R_{23}\,\Omega_{23}\right)\right) \tag{13}$$

$$\mathcal{P}_{33} = 2\left(kS_{33}/A_1 + \left(R_{23}\,\Omega_{23} - R_{31}\,\Omega_{31}\right)\right) \tag{14}$$

With corresponding off diagonal terms

$$\mathcal{P}_{12} = 2kS_{12}/A_1 + \left(R_{23}\,\Omega_{31} - R_{31}\,\Omega_{23} + \left(R_{11} - R_{22}\right)\Omega_{12}\right) \tag{15}$$

$$\mathcal{P}_{23} = 2kS_{23}/A_1 + \left(R_{31}\,\Omega_{12} - R_{12}\,\Omega_{31} + \left(R_{22} - R_{33}\right)\Omega_{23}\right) \tag{16}$$

$$\mathcal{P}_{31} = 2kS_{31}/A_1 + \left(R_{12}\,\Omega_{23} - R_{23}\,\Omega_{12} + \left(R_{33} - R_{11}\right)\Omega_{31}\right) \tag{17}$$

These then provide the equilibrium Reynolds stress using Eq. 18

$$R_{ij}{}^{(eq)} = \frac{2}{3}k\delta_{ij} - \frac{A_1}{\omega}\left(\mathcal{P}_{ij} - \frac{1}{3}\bar{\mathcal{P}}\delta_{ij}\right) + \frac{1}{A_0\rho\omega}\left[\partial_l\left(\left(\mu + \sigma_r\mu_T\right)\partial_l R_{ij}\right) - A_3\partial_l\left(\rho T_{ijl}\right)\right] \tag{18}$$

The other model parameters are:

$$\begin{array}{llllll} A_0 = & 1.0 & \alpha = & 0.35 & & \\ A_1 = & \frac{5}{3} & \beta = & 0.1 & \sigma_k = 0.3 & \sigma_r = 0.0 \\ A_2 = & 1.0 & \beta^* = & 0.12 & \sigma_\omega = 0.3 & \sigma_t = 0.0 \end{array}$$

Note that even though $\beta$ and $\beta^*$ have been altered from the 1988 $k$-$\omega$ choices, their ratio is retained providing the same isotropic turbulence decay rate.

Two special parameter choices are used to elucidate the coupling and effect of the $T_{ijk}$ terms. The first parameter choice $A_3 = A_4 = 0$ is labelled as "Uncoupled" in the flat plate results, and will produce Reynolds-stresses identical to the original Reynolds stress models, along with the turbulent transport terms $T_{ijk}$ that are consistent with those $R_{ij}$ predictions. The second special parameter choice $A_3 = 1$, $A_4 = 0$ is labelled as "PC"(Partially Coupled), and these include the $T_{ijk}$ terms in the Reynolds stress equations, but do use only the gradient transport term for the equilibrium $k$ equation turbulent transport. As the equations drive the predicted $k$ toward the $k^{eq}$, this version is missing the direct influence of what should be improved turbulent transport predictions for the evolution of the turbulent kinetic energy. As neither of these choices uses the new model for the turbulent transport in the $k$ equation, for both of these special parameter sets $\sigma_k = 0.8$, the value used with Reynolds-stress model on which the coupled model is based.

The equations set with $A_3 = 1, A_4 = 1$ is labelled as "TTR" in the figures, and these use the triple product terms to provide part of the turbulent transport. As such, a reduced $\sigma_k = 0.3$ is used (which was 0.2 in the paper introducing the model), where the other less coupled parameter choices have $\sigma_k = 0.8$. The change in $\sigma_k$ was due to experience gained in simulating the rotating pipe case, and this change is being investigated for it's effect on the flows in that paper. So far, the change has not introduced any large differences in those results. This parameter choice is the current version of the triple product turbulent transport model (TTR), and expected to be the final model definition. A full exploration focusing on separated flowfields is planned, and that paper will include a full comparison on a wide selection of flowfields, with an emphasis on separation and reattachment predictions.

## Appendix B Solution Sensitivity Assessment

Matching the incompressible results achieved in an incompressible solver[14] proved more challenging than anticipated. As the end product of this effort was to provide a simple flowfield that could be used as a test case for rotation/curvature corrections, eliminating discrepancies between the simulations, and assessing sensitivity to simulation choices was necessary.

Other possible factors affecting the solution were assessed, and were all very small compared to the radial coarsening sensitivity, with smoothing parameters for the matrix dissipation (eigenvalue limiters set to zero), use of the HLLC upwind method, solution of the flowfield at a relative Mach number that did not require preconditioning, solution of the flowfield at a Reynolds number higher by a factor of 10 (with a suitably radially clustered grid which had a similar initial $\Delta y^+$ ) showed these all these factors to be non-issues, at least with the radial grid density chosen.

The method used to obtain a solution with $Re_\tau = 875$ in the non rotating section was to obtain successive solutions for a given downstream pressures, adjusting the downstream pressure to raise or lower the value to match the desired $Re_\tau = 875$. An alternative method is to choose a back pressure, then adjust the global Reynolds number parameter (REY = $\frac{\rho_\infty u_\infty R}{\mu_\infty}$) of OVERFLOW. Solutions obtained by these two methods give identical results in non-dimensional coordinates for the test case axisymmetric grids. This match of solutions gave confidence that the simulations with

either method were providing the unique answer to the boundary value problem when expressed in non-dimensional terms.

For the grid density chosen the centerline value in the non-rotating, fully developed pipe flow region is $u_0/u_\tau = 21.25$ for the SST model. From grid density studies for an axisymmetric version of the grid, a grid with twice the density in both directions would give 21.56 for this value, and with a radial density of 900 points, this becomes 21.63.

## References


[1]Pope, Stephen B., *Turbulent Flows*, Cambridge University Press, 2000.

[2]Wilcox, David C., *Turbulence Modeling for CFD*, DCW Industries, Inc, 2006.

[3]Gerolymos, G.A., Joly, S., Mallet, M., and Vallet, I, "Reynolds-Stress Model Flow Prediction in Aircraft-Engine Intake Double-S-Shaped Duct," *Journal of Aircraft*, Vol. 47, No. 4, July-August 2010, pp. 1368–1381.

[4]Cecora, Rene-Daniel, Eisfeld, Bernhard, Probst, Axel, Crippa, Simone, and Radspiel, Rolf, "Differential Reynolds Stress Modeling for Aeronautics," AIAA Paper 2012-0465.

[5]Randolph Lillard, Brandon Oliver, Michael Olsen, G. A. Blaisdell, and A. S. Lyrintzis, "The LagRST Model: a Turbulence Model for Non-Equilibrium Flows," AIAA Paper 2012-444.

[6]Olsen, M. E. , Lillard, R. P., and Murman S. M., "Separation Prediction of Large Separations with Reynolds Stress Models," AIAA Paper 2013-2720.

[7]Olsen, Michael E, "Prediction of Large Separations with a Third-Order-Moment Model," AIAA Paper 2015-1968.

[8]Zaets, P., Onufriev, A., Safarov, N., and Safarov, R., "Experimental study of the behavior of the energy spectrum in a turbulent flow in a tube rotating relative to its longitudinal axis," *Journal of Applied Mechanics and Technical Physics*, Vol. 33, No. 1, 1992, pp. 31–35.

[9]Kurbatskii, A. and Poroseva, S., "Modeling turbulent diffusion in a rotating cylindrical pipe flow," *International Journal of Heat and Fluid Flow*, Vol. 20, No. 3, 1999, pp. 341 – 348.

[10]Reich, G. and Beer, H., "Fluid flow and heat transfer in an axially rotating pipeI. Effect of rotation on turbulent pipe flow," *International Journal of Heat and Mass Transfer*, Vol. 32, No. 3, 1989, pp. 551 – 562.

[11]Nishibori, K., Kikuyama, K., and Murakami, M., "Laminarization of Turbulent Flow in the Inlet Region of an Axially Rotating Pipe : Fluids Engineering," *JSME international journal*, Vol. 30, No. 260, 1987, pp. 255–262.

[12]Chow, Jim, Zilliac, Greg, and Bradshaw, Peter, "Turbulence Measurements in the Near Field of a Wingtip Vortex," NASA TM 110418.

[13]Olsen, M. E., Lillard, R. P., and Coakley, T., "LagRST Model Predictions of a Wingtip Vortex Flowfield (Invited)," AIAA Paper 2015-2923.

[14]Ashton, Neil, "Computation of Turbulent Flow in a Rotating Pipe using standard eddy-viscosity models and an Elliptic Blending Reynolds Stress Model," AIAA Paper 2016-XXXX, (Companion paper in session).

[15]Rumsey, C., "Langley Research Center Turbulence Modeling Resource," March 2015, [Online; accessed 6-May-2016].

[16]Zaets, P. G., Onufriev, A. T., Safarov, N. A., and Safarov, R. A., "Experimental study of spectra corresponding to friction stress and the third statistical moments in fully developed turbulent pipe flow," *Journal of Applied Mechanics and Technical Physics*, Vol. 35, No. 6, 1994, pp. 906–910.

[17]Zaets, P. G., Onufriev, A. T., Pilipchuk, M. I., Safarov, N. A., and Safarov, R. A., "Experimental study of the behavior of quadruple time correlation functions for the longitudinal velocity fluctuation in developed turbulent pipe flow," *Journal of Applied Mechanics and Technical Physics*, Vol. 37, No. 5, 1996, pp. 617–621.

[18]Zaets, P. G., Kurbatskii, A. F., Onufriev, A. T., Poroseva, S. V., Safarov, N. A., Safarov, R. A., and Yakovenko, S. N., "Experimental study and mathematical simulation of the characteristics of a turbulent flow in a straight circular pipe rotating about its longitudinal axis," *Journal of Applied Mechanics and Technical Physics*, Vol. 39, No. 2, 1998, pp. 249–260.

[19]Bardina, J. E., Huang, P. G., and Coakley, T., "Turbulence Modeling Validation, Testing, and Development," NASA TM 110446.

[20]Buning, P., Jespersen, D., Pulliam, T., Klopfer, G., Chan, W., Slotnick, J., Krist, S., and Renze, K., *OVERFLOW User's Manual, Version 1.8s*, NASA Langley Research Center, 2000.

[21]Pulliam, D. J. T. H. and Buning, P. G., "Recent Enhancements to OVERFLOW," AIAA Paper 97-0664.

[22]Olsen, Michael E. and Prabhu, D. K., "Application of OVERFLOW to Hypersonic Perfect Gas Flowfields," AIAA Paper 2001-2664.

[23]Swanson, R. C. and Turkel, E., "On Central–Difference and Upwind Schemes," *Journal of Computational Physics*, Vol. 101, 1992, pp. 292–306.

[24]Nichols, R. H., Tramel, R. W., and Buning, P. G., "Evaluation of two high-order weighted essentially nonoscillatory schemes," *AIAA journal*, Vol. 46, No. 12, 2008, pp. 3090–3102.

[25]Pulliam, T. H., "High order accurate finite-difference methods: as seen in OVERFLOW," AIAA Paper 2011-3851.

[26]Pulliam, T. and Chaussee, D., "A diagonal form of an implicit approximate-factorization algorithm," *Journal of Computational Physics*, Vol. 39, No. 2, 1981, pp. 347 – 363.

[27]Potsdam, M., Sankaran, V., and Pandya, S., chap. Unsteady Low Mach Preconditioning with Application to Rotorcraft Flows, Fluid Dynamics and Co-located Conferences, American Institute of Aeronautics and Astronautics, Jun 2007, 0.

[28]Smits, A. J., McKeon, B. J., and Marusic, I., "HighReynolds Number Wall Turbulence," *Annual Review of Fluid Mechanics*, Vol. 43, No. 1, 2011, pp. 353–375.

[29]Hultmark, M., Vallikivi, M, Bailey, S.C.C., and Smits, A.J., "Logarithmic scaling of turbulence in smooth and rough-wall pipe flow," *Journal of Fluid Mechanics*, Vol. 728, 2013, pp. 376–395.

[30]Vallikivi, M, Hultmark, M., and Smits, A.J., "Turbulent boundary layer statistics at very high Reynolds number," *Journal of Fluid Mechanics*, 2014, Under Review for Publication.

[31]DeGraaff, David B. and Eaton, John K., "Reynolds-number scaling of the flat-plate turbulent boundary layer," *Journal of Fluid Mechanics*, Vol. 422, 2000, pp. 319–322.

[32]Dussauge, J.P., Smith, R.W., Smits, A.J., Fernhoz, H., Finley, P.J., and Spina, Eric F., "Turbulent Boundary Layers in Subsonic and Supersonic Flow," AGARDOGRAPH 335.

[33]Olsen, M. E., "Prediction of Separation with a Third-Order-Moment Model," AIAA Paper 2015-1968.

[34]Olsen, M. E. , Lillard, R. P., and Coakley T. J., "The Lag Model Applied to High Speed Flows," AIAA Paper 2005-101.

[35]Mani, M., Babcock, D., Winkler, C., and Spalart, P., chap. Predictions of a Supersonic Turbulent Flow in a Square Duct, Aerospace Sciences Meetings, American Institute of Aeronautics and Astronautics, Jan 2013, 0.

[36]Shur, Michael L., Strelets, Michael K., Travin, Andrey K., and Spalart, Phillipe R., "Turbulence Modeling in Rotating and Curved Channels: Assessing the Spalart-Shur Correction," *AIAA Journal*, Vol. 38, No. 5, 2000, pp. 784–792.

[37]Childs, Marisssa L., Pulliam, Thomas H., and Jespersen, Dennis C., "OVERFLOW Turbulence Model Resource Verification Results," NAS Technical Report 2014-03, NASA, June 2014, NAS Technical Report NAS-2014-03.

[38]Bissonnette, L. R. and Mellor, G. L., "Experiments on the behaviour of an axisymmetric turbulent boundary layer with a sudden circumferential strain," *Journal of Fluid Mechanics*, Vol. 63, 4 1974, pp. 369–413.

[39]Driver, D. M. and Hebbar, S. K., "Experimental study of a three-dimensional, shear-driven, turbulent boundary layer," *AIAA Journal*, Vol. 25, No. 1, Jan 1987, pp. 35–42.

[40]Higuchi, H. and Rubesin, M. W., "Behavior of a Turbulent Boundary Layer Subjected to Sudden Transverse Strain," *AIAA Journal*, Vol. 17, No. 9, Sep 1979, pp. 931–941.

[41]Pope, S., "A more general effective-viscosity hypothesis," *Journal of Fluid Mechanics*, Vol. 72 (part 2), 1975, pp. 331–340.

[42]Wallin, Stefan and Johansson, Arne V., "An explicit algebraic Reynolds stress model for incompressible and compressible flows," *Journal of Fluid Mechanics*, Vol. 403, 2000, pp. 89–132.

[43]Hellsten, Antti, *New two equation Turbulence Model for Aerodynamic Applications*, Ph.D. thesis, Helsinki University of Technology, February 2004.

[44]Townsend, A.A., *"The structure of turbulent shear flow"*, Cambridge University Press, 2nd ed., 1976.